A Model for Human–Human Collaborative Object Manipulation and Its Application to Human–Robot Interaction

Ehsan Noohi, Miloš Žefran, and James L. Patton

***Abstract*—During collaborative object manipulation, the interaction forces provide a communication channel through which humans coordinate their actions. In order for the robots to engage in physical collaboration with humans, it is necessary to understand this coordination process. Unfortunately, there is no intrinsic way to define the interaction forces. In this study, we propose a model that allows us to compute the interaction force during a dyadic cooperative object manipulation task. The model is derived directly from the existing theories on human arm movements. The results of a user study with 22 human subjects prove the validity of the proposed model. The model is then embedded in a control strategy that enables the robot to engage in a cooperative task with a human. The performance evaluation of the controller through simulation shows that the control strategy is a promising candidate for a cooperative human–robot interaction.**

***Index Terms*—Cooperation strategy, dyadic object manipulation, human–human cooperation, interaction force, physical human–robot interaction (pHRI).**

I. Introduction

MANY robotic applications require proactive physical interaction between a human and a robot. For instance, consider a robotic caregiver in the elderly care application. It has been shown that home care aides are most effective when they actively involve the elderly in physical activities [1], [2]. That is, it is important that the caregiver does not simply perform the task for the elder person, the elderly should be asked to proactively contribute in performing the task. Cooperative object manipulation (e.g., moving a table) is another example of when proactive interaction is necessary. In general, in cases of cooperative physical interaction, successful completion of the task requires a coordinated force exchange between the human and the robot.

Manuscript received February 02, 2016; accepted April 17, 2016. Date of publication August 05, 2016; date of current version August 18, 2016. This paper was recommended for publication by Editor A. Kheddar and Guest Editors D. Kulic and G. Venture upon evaluation of the reviewers' comments. This work was supported by the National Science Foundation under Grant IIS-0905593, Grant CNS-0910988, and Grant CNS-1035914.

E. Noohi is with the Robotics Laboratory, Department of Electrical and Computer Engineering, University of Illinois at Chicago, Chicago, IL, USA, and also with the Robotics Laboratory, Rehabilitation Institute of Chicago, Chicago, IL, USA (e-mail: enoohi2@uic.edu).

M. Žefran is with the Robotics Laboratory, Department of Electrical and Computer Engineering, University of Illinois at Chicago, Chicago, IL, USA (e-mail: mzefran@uic.edu).

J. L. Patton is with the Sensory Motor Performance Program, Rehabilitation Institute of Chicago, Chicago, IL, USA, and also with the Bioengineering Department, University of Illinois at Chicago, Chicago, IL, USA (e-mail: pattonj@uic.edu).

Color versions of one or more of the figures in this paper are available online at http://ieeexplore.ieee.org.

Digital Object Identifier 10.1109/TRO.2016.2572698

While the human can usually amplify the cooperation performance by adjusting to the robot's actions, in many applications the human is not capable of such an adjustment. For instance, in elderly care, rehabilitation, or childcare, the human is either an elderly person, a physically challenged patient, or a toddler. In such applications, the human is not expected to adjust to the robot. Instead, the robot's actions need to be as natural to the human as possible. Therefore, modeling the characteristics of natural human movements and the properties of the exchanged forces would significantly contribute to designing better robot control strategies in such applications.

In order to build a model for a natural (human-like) interaction, researchers have studied human–human collaborative tasks and proposed different models for the exchanged forces between humans. However, due to the physics of the task, there is an inherent ambiguity in trying to recover the interaction forces from the forces exerted by the humans. In other words, since the interaction force (the portion of the applied force that does not contribute to the motion of the object) is unknown, obtaining the effective portion of the applied force for each individual is challenging. To resolve this ambiguity, different models for the interaction force have been proposed [3]–[7]. In all of these models (including ours), the ambiguity is resolved by introducing additional constraints in the interaction model. For instance, Williams and Khatib [3] suggest that the interaction force follows the mechanical internal force. Groten *et al.* [4] assume that the human minimizes the energy of the interaction force during the collaboration. Some of the suggested constraints cannot be used in a cooperative collaboration setting. The leader/follower scheme [5] is an example of such constraints. Some other models have also been proposed, but they are not applicable in an online physical human-robot interaction setup, as they only provide a descriptive model for an existing interaction (e.g., [6]). We will discuss the properties of these models in more detail in Section III-D.

The existing models compute the interaction force for every isolated pair of force vectors and ignore the time dependencies among the force pairs during the task. In contrast, our approach considers the entire trajectories of the force vectors to compute the interaction force. More specifically, the interaction force is obtained by exploiting a computational motion model of the nominal movement trajectory during the cooperation. In fact, the knowledge of the motion model serves as the constraint that resolves the ambiguity.

Our contribution is threefold. First, by exploiting the motion model associated with the task, we propose a descriptive model

for the interaction force. The key advantage of the proposed model compared with other models is that it only requires one of the applied forces to be measured in order to compute the interaction force. As a result, during a human–robot collaborative task, the robot can model the interaction force by measuring only the force applied by the human. In turn, this significantly simplifies the robot's controller. Details are given in Section IV.

Second, we propose a controller for the robot that exploits the interaction force model to determine the force that the robot should apply. While the robot is aware of the task, the human's desired trajectory is unknown to the robot. Using the interaction force information, the controller responds to the human's applied force in such a way that the human's desired trajectory can be followed. We refer to this controller as the offline controller, because the interaction force is computed offline. In Section VII we statistically analyze the performance of the controller with and without the interaction force information. We show that the performance is significantly higher statistically when the interaction force information is provided.

Finally, we propose an online controller for the robot that exploits a real-time estimation of the interaction force. The estimation algorithm is based on our proposed model. It also utilizes a predication of the human's future actions. In Section VIII we introduce the online controller in detail and compare it with the offline controller in simulation. We show that no statistically significant difference exists in the performance of the two controllers in these simulations.

The rest of the paper is organized as follows. In Section II we discuss the relevant literature on the models for the human-arm movement and on the human–robot interaction. In Section III we review the models of the arm movement that will be used in the paper and introduce the necessary background on modeling forces during cooperative manipulation. Our model for the interaction force is introduced in Section IV. To evaluate the model, we conducted a human study with 22 subjects. The study considers both dyadic (two-person) manipulation and single-person bimanual (SPB) manipulation. The experimental setup is described in Section V. Using the collected data, we compare the performance of our model with two existing descriptive models in Section VI. In particular, we show that the proposed model can distinguish between the dyadic manipulation and the bimanual manipulation. In Section VII we investigate the effect of the interaction force on the performance of the robot. We show that providing the robot with the interaction force (computed offline) significantly improves its performance. By further exploiting the properties of our model we construct an interaction force estimator in Section VIII. The estimator is then incorporated into an impedance controller that implements the cooperation strategy for the robot. Finally, we present the performance evaluation that demonstrates the effectiveness of the proposed controller.

II. Related Work

Human movement has been studied extensively. While formulating a model that accounts for trial-to-trial variations of the motion trajectory is a challenging research problem, the average motion trajectory has been successfully described with several models. It has been shown that many biological movement profiles exhibit certain regularities. In a large class of complex movements, e.g., drawing a curved path, Lacquaniti *et al.* [8] showed that the angular velocity and the path curvature are in a power relation, referred to as the two-third power law. In grasping and reaching movements, Fitts [9] showed that a linear relation exists between the movement time and the index of difficulty (defined in terms of the distance to the target and the size of the target).

A number of successful models for biological movements have been proposed that are based on optimal control [10]. These models suggest that the human sensorimotor system optimizes a certain cost function in order to perform specific movements. Anderson and Pandy [11] showed that metabolic energy minimization reproduces the salient features of normal gait (for walking on level ground). Flash and Hogan [12] showed that a minimum-jerk model accurately describes trajectories of the reaching movements. This model generates the well-known bell-shaped velocity profile and can describe the relation between the velocity and the curvature even more accurately than the two-third power law [10]. The minimum torque change model has been proposed as an alternative to the minimum-jerk model [13], [14]. In this model, the nonlinear dynamics of the arm is considered and the motion trajectory is obtained by minimizing the variations of the applied joint torques. The accuracy of the final position (with respect to the target point) is proposed as another optimization criterion. Harris and Wolpert [15] suggested that the optimal trajectory minimizes the final position variance, also known as the minimum variance model. The model is shown to be very successful in describing speed profiles of saccadic eye movements and is consistent with both Fitts' law and the power law.

While there exists a rich literature on modeling single arm reaching movements, bimanual and dyadic movements are studied less. Tresilian and Stelmach [16] showed that the aperture and transport components of a single-arm reach-to-grasp task is very similar to the bimanual performance of the same task. Garvin *et al.* [17] studied the bimanual reaching movement and proposed an extension to the minimum-jerk model by incorporating the rotational jerk of the object into the optimization criterion. Diedrichsen [18] studied bimanual reaching movement in one-cursor and two-cursor conditions and showed that the change in the control and in the adaptation are both optimal and task dependent. Noohi *et al.* [19] have recently shown that the object's motion trajectory during the bimanual and dyadic reaching movements is highly correlated with the minimum-jerk trajectory.

In addition to the motion trajectory, the cooperation aspect of dyadic and bimanual movements has been studied as well. The exchanged forces have been shown to convey rich information about the cooperation [20]. Many researchers have studied the haptic clues as a communication channel that facilitates the physical interaction. Guiard [21] suggested that in bimanual tasks, while one arm performs the majority of the workload, the other arm is responsible for fine tuning and corrections. Reed *et al.* [22] observed similar arm specialization in a dyadic task in which one person is contributing more to the acceleration and

the other person to the deceleration. Noohi and Žefran [23] characterized the dyadic object manipulation task and proposed a set of measures that evaluate the performance of haptically coupled subjects and cross-validated those metrics with the subjects' self-assessments. Groten *et al.* [24] suggested that, in a shared decision making situation, the haptic channel enhances the intention integration and results in a higher performance. Ganesh *et al.* [25] reported that haptically coupled subjects demonstrate better motor performance than a single person in a virtual pursuit-tracking task. van der Wel *et al.* [26] show that, in an object manipulation task, dyads amplify their applied forces to develop a haptic communication channel. Mörtl *et al.* [27] studied the process of role assignment (leader/follower roles) during the physical cooperation. Feth *et al.* [28] studied a joint-pursuit-tracking task and observed that the performance of a dyadic collaboration is higher than for single individuals. Based on the asymmetry of energy flow between the subjects, they suggested that the increased performance was due to the emergence of different roles. Sawers and Ting [29] have recently provided a thorough review on this topic, while focusing on the design of rehabilitation robots.

Many of these models have been adopted by researchers in assistive and rehabilitation applications in order to improve the performance of the physical interaction between a robot and a human. For instance, Corteville *et al.* [30] proposed an admittance control scheme for fast point-to-point cooperative sliding of an object. The controller takes advantage of an extended Kalman filter to estimate the parameters of the motion velocity. The velocity profile was assumed to follow the minimum-jerk model. Bussy *et al.* [31] proposed motion primitives for cooperative transportation of heavy objects and introduced a velocity-based algorithm to generate a sequence of such proposed primitive motions. Medina *et al.* [32] proposed a risk-sensitive optimal controller that responds to the uncertainty in the predicted human motion by adapting the robot's role. They modeled the human as a process noise that the robot needs to consider in its optimization cost function.

III. Background

A. Motion Trajectory During Reaching Movement

Reaching movement is one of the well-studied human motions. In this motion, a person moves his/her hand from point A to point B in a straight line. The motion is fast and happens over a short distance. When performing the single arm reaching movement, it has been shown that humans generate a smooth trajectory with the well-known bell-shaped curve for hand velocity [12]. More specifically, the hand trajectory minimizes the following cost function:

$$H(t_i, t_f, x) = \frac{1}{2}\int_{t_i}^{t_f} \left\| \frac{\mathrm{d}^3 x(t)}{\mathrm{d}t^3} \right\|^2 dt$$
$$x^*(t) = \underset{x(t)}{\operatorname{argmin}} \left(H(t_i, t_f, x) \right) \quad (1)$$

where $x(t)$ is the position trajectory of the hand, t_i is the start time of the motion, and t_f is the end time. If we take the assumption that the hand is at rest at the start and at the end of the reaching movement (i.e., zero boundary conditions), the minimum of the cost function would be $H^* = 360L^2$ and the optimal trajectory is $x^*(\tau) = x_i + L(6\tau^5 - 15\tau^4 + 10\tau^3)$. Here, $\tau = (t - t_i)/(t_f - t_i)$ and $L = \|x_f - x_i\|$. In addition, $x_i = x(t_i)$ and $x_f = x(t_f)$ are the positions of the hand at the start point and the end point, respectively. Since the cost function is the sum of the squared jerk along the motion trajectory, this model is referred to as the *minimum-jerk* trajectory hereafter.

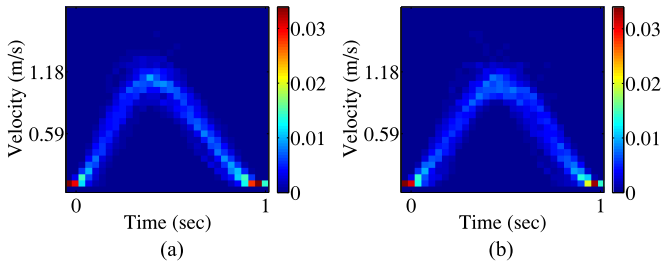

Fig. 1. 2-D histogram of normalized object velocities for bimanual and dyadic object manipulation during a reaching movement task. The color of each bin represents the percentage of the samples observed in that bin. (a) SPB, (b) dyadic cooperation.

B. Motion Trajectory of Dyadic Reaching Movement

In a bimanual object manipulation, the object is grasped by two hands and is moved from a starting point to an ending point. In SPB manipulation (in which both hands belong to the same person), it has been shown that the object closely follows an optimal trajectory [17]. That's due to the fact that both hands receive synchronized commands from a common controller (a person's brain). Bilateral training methods in rehabilitation exploit this feature and significant improvements in patients with poststroke hemiparesis have been reported [33].

In a dyadic reaching movement, however, the imperfect synchronization between the two cooperating persons can introduce deviation from the optimal trajectory. That is, although the motion's start point (x_i) and end point (x_f) are known, the persons' estimation/control of their hands' positions are different. More importantly, each person has his/her own preferred speed. We have recently shown that the object's motion trajectory during the dyadic reaching movement is highly correlated with the minimum-jerk trajectory [19]. More specifically, the Pearson correlation coefficient between the normalized object velocity and the velocity profile of a minimum-jerk trajectory is $\hat{\rho} = 0.97$ with $CI_{95\%} = [0.95, 0.98]$.

Fig. 1 shows the 2-D histogram of normalized object velocities that are recorded during SPB and dyadic reaching movement [19]. The velocities are normalized both in time (scaled to 1 s) and in traveled distance (scaled to 1 m). Since the number of trials was different in SPB and dyadic modes, the histogram reports the percentage of observed values. In other words, in each mode, the number of observed samples in each bin is divided by the total number of the samples in that mode. For more details please refer to [19].

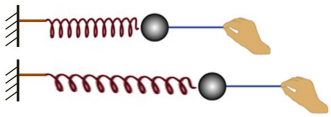

Fig. 2. Reaching movement under a spring-like force field.

C. Applied Force During Reaching Movement

Disturbing the reaching movement by an external force field will deviate the hand trajectory from its optimal trajectory. It has been shown that, after enough learning trials, humans can adapt to the external force field and return to their original trajectories [34]–[36]. Consider the situation in which a subject performs a reaching movement while a spring resists his/her forces (see Fig. 2). The spring introduces the position-dependent force field $F = -k_s\,(x(t) - x_0)$, where k_s is the stiffness of the spring and, x_0 is the position of the spring's end when no force is applied to it. After the adaptation period, the subject learns to cancel the force field and returns to the optimal trajectory, $x^*(t)$, for the reaching movement [35]. More interestingly, the force that the subject needs to apply at the end effector (to cancel the force field) is $F^*(t) = -k_s\,(x^*(t) - x_0)$. In other words, the applied force follows a smooth minimum-jerk trajectory. Since $\mathrm{d}^3x(t)/\mathrm{d}t^3 = (-k_s^{-1})\,\mathrm{d}^3F(t)/\mathrm{d}t^3$, we can rewrite (1) as

$$F^*(t) = \underset{F}{\operatorname{argmin}} \left(\frac{1}{2} \int_{t_i}^{t_f} \left\| \frac{\mathrm{d}^3F(t)}{\mathrm{d}t^3} \right\|^2 \mathrm{d}t \right). \tag{2}$$

Equation (2) states that, in a *spring-like force field*, the applied force minimizes the squared-jerk cost function. Applying the calculus of variations techniques on (2), it is easy to show that the sixth derivative of $F^*(t)$ is zero [37]. Therefore, the applied force can be represented as a fifth-order polynomial as

$$F^*(t) = \sum_{k=0}^{5} c_k t^k. \tag{3}$$

Note that, if the hand is at rest at the start and at the end of the reaching movement, the applied forces are, too. In the general case that the hand is not at rest, to determine the c_k coefficients in (3) the minimization problem of (2) should satisfy the boundary conditions.

D. Models for the Interaction Force

Consider a dyadic object manipulation task. Let f_1 and f_2 refer to the forces that are applied to the manipulated object and $F_{\text{sum}} = f_1 + f_2$ be the resultant force that is associated with the task. Each applied force can be decomposed into the effective force (f_1^* and f_2^*) and the interaction force (F^i) as

$$\begin{aligned} f_1 &= f_1^* + F^i \\ f_2 &= f_2^* - F^i. \end{aligned} \tag{4}$$

The interaction force can be used to secure the grasp or to communicate with the other person [26], [38]. It can compress or stretch the object, but it does not influence the object's equations of motion. As a result, all force components that lie in the null space of F_{sum} (orthogonal to it) are part of the interaction force. That is

$$\begin{aligned} f_1^* &= \alpha F_{\text{sum}} \\ f_2^* &= (1-\alpha) F_{\text{sum}} \end{aligned} \tag{5}$$

and, therefore,

$$F^i = (1-\alpha) f_1 - \alpha f_2 \tag{6}$$

where α denotes the contribution of each person in performing the task.

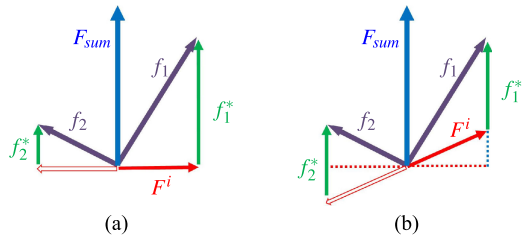

Fig. 3. For a single pair of forces, f_1 and f_2, the orthogonal (a) and nonorthogonal (b) decompositions are illustrated. Note that the orthogonal decomposition matches the ME model and the nonorthogonal decomposition matches the VL model.

Note that (4) is an underdetermined system of equations and that any arbitrary value of α $(0 \le \alpha \le 1)$ introduces a valid decomposition. According to (5) and (6), the only situation in which the system has a unique solution is when $F_{\text{sum}} = 0$. In such instances, $F^i = f_1 = -f_2$ and $f_1^* = f_2^* = 0$. In all other situations, to be able to uniquely determine the interaction force, one needs to introduce an additional constraint to the system (e.g., introducing specific values for α). Note that we take the general case in which both hands can apply pure torque to the object and, thus, the direction of the interaction force is not necessarily aligned with the grasp configuration (no additional torque constraints).

Fig. 3 shows two possible decomposition examples for a single pair of applied forces. Note that in Fig 3(b) the interaction force has both orthogonal and parallel components (w.r.t. F_{sum}). While obtaining the orthogonal component is straightforward, finding a computational model for the parallel component is challenging. That is the reason we only focus on the parallel components of f_1, f_2, and F^i in this study. We will refer to these parallel components as the applied forces (f_1 and f_2) and interaction force (F^i) hereafter. After the interaction force is computed, it will be augmented with the orthogonal component.

To uniquely determine the interaction force, researchers have considered different approaches. In the case of the human–robot collaboration, some researchers tackle this problem by assigning leader/follower roles to the human and the robot ($\alpha = 0$ or $\alpha = 1$), e.g., [5]. Mörtl *et al.* [27] studied the exchange of the leader/follower roles between the human and the robot, and observed that dynamic role assignments resulted in a considerably larger interaction force. Evrard and Kheddar [6] suggested that a continuous homotopy switching happens between the leader and the follower roles during the collaboration

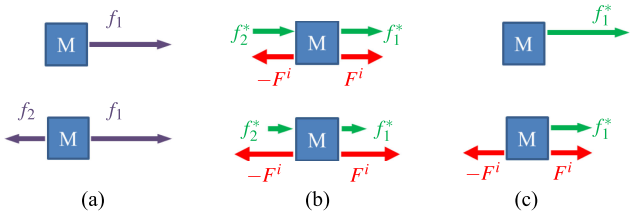

Fig. 4. (a) Force decomposition of the applied forces, based on (b) the VL model and (c) the ME model. Note that when only one force acts on the object, the ME model suggests zero interaction force, while VL model does not. (a) Applied forces, (b) VL, (c) ME. (a) Applied forces, (b) VL, (c) ME.

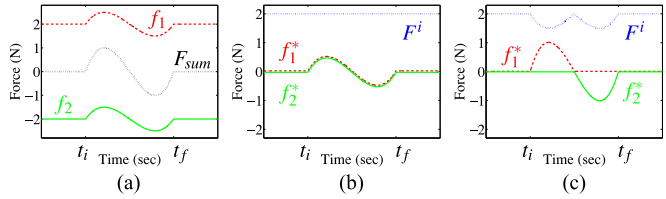

Fig. 5. Comparison on different assumptions in a 1-D object manipulation task. (a) Applied forces and the total force. (b) VL assumption. (c) ME assumption. In both (b) and (c), f_1^*, f_2^*, and F^i are dashed, solid, and dotted lines, respectively.

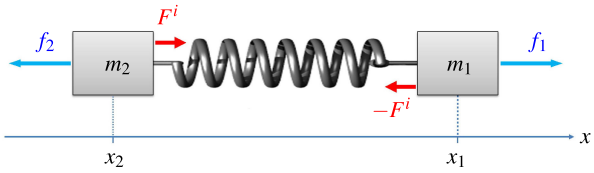

Fig. 6. Mass-spring system in a cooperative manipulation task. The spring is assumed to be massless and linear. The force f_1 (f_2) is applied to the mass m_1 (m_2). The position of the center of mass m_1 (m_2) is x_1 (x_2). The system is one-dimensional; that is, applied forces are parallel with the x-axis.

(for each agent independently). However, they did not identify the homotopy function for dyadic tasks. Leader/follower schemes are very successful in the tasks in which the human steers the task and the robot provides the whole workload and follows the human.

Unlike leader/follower schemes, in this study we are interested in cooperative object manipulation task in which both human and robot are actively contributing in performing the task. One of the most appreciated approaches is to take the mechanical internal force as the interaction force. For instance, while proposing a hybrid position/force control scheme for two coordinated robots, Uchiyama and Dauchez [39] described the interaction between the robots by the internal force/moment vector. Using this vector, the authors manage to describe the object deformation (including twisting, bending, and shearing) during manipulation. Williams and Khatib [3] introduced a more general framework to properly design the interaction forces for multicontact robot–robot collaborative tasks, namely the *virtual linkage* (VL) model. They suggested that an acceptable interaction force would minimize the *engineering strain* (minimum deformation of the object). They used the internal forces as the interaction force in multirobot object manipulation. In the case of two robots, the force decomposition would become

$$f_1^* = f_2^* = \frac{1}{2}F_{\text{sum}}$$
$$F^i = \frac{1}{2}(f_1 - f_2) \tag{7}$$

or $\alpha = 0.5$. Taking the difference of the applied forces as the interaction force, as expressed in (7), is a common practice in the human–robot interaction literature as well, e.g., [7].

Another interesting assumption in the literature, proposed by Groten *et al.* [4], is that a human minimizes the energy of the interaction force during the collaboration. They studied the dominance distribution in a dyadic haptic collaboration and implicitly exploited the minimum-energy (ME) model. The assumption is based on the intuition that when only one force is applied to an object, the interaction force should be zero. Fig. 4 illustrates this intuitive assumption in comparison with the VL model. This model finds a solution for (5) and (6) in which the magnitude of the interaction force is minimum. In other words

$$\alpha(t) = \underset{\alpha}{\text{argmin}} \left(||F^i|| \right). \tag{8}$$

Fig. 5(a) shows a typical example of a bimanual object manipulation in 1-D. The interaction force before the start of the motion ($t \leq t_i$) and after the end of the motion ($t \geq t_f$) is $F^i = 2$, which is the grasp force to hold the object. Fig. 5(b) shows the interaction force and the effective forces obtained from VL model. Here, $F^i = 2$ and $f_1^* = f_2^* = \frac{1}{2}F_{\text{sum}}$. The model suggest a perfect load-sharing cooperation, which is a likely behavior in a SPB manipulation. Fig. 5(c) depicts the interaction force and the effective forces based on the ME assumption. Under this assumption, the first (second) hand applies the whole required force (F_{sum}) to move the object in the acceleration (deceleration) phase of the manipulation, while the other hand applies zero force (ZF). Taking the accelerating/decelerating roles is an expected behavior in dyadic collaborative tasks [22]. We will compare our proposed model with these two models in the following sections.

IV. Proposed Model for the Interaction Force

In this section we first compute the interaction force in a mass-spring system and then discuss how a mass-spring system generalizes a rigid body model for a solid body. Next, we propose our model for the interaction force, using the knowledge of the task. Finally, we discuss different aspects of the proposed model and list its key features.

A. Interaction Force in a Mass-Spring System

Consider the cooperative manipulation of the mass-spring system in Fig. 6. The masses m_1 and m_2 are coupled with a spring and the forces f_1 and f_2 are applied to them, respectively. The positions of the masses m_1 and m_2 are referred to by x_1 and x_2 ($x_1 > x_2$), respectively. The task is to move the masses from their initial configurations (x_{i_1} and x_{i_2}) to the goal

configurations (x_{f_1} and x_{f_2}) on a straight line (aligned with the x-axis).

If the position variables are available (or can be measured), the interaction force that the spring introduces to the system is computed as

$$F^i(t) = -k_s\,(x_1(t) - x_2(t) - L_0) \tag{9}$$

where k_s is the stiffness of the spring and L_0 is the length of the spring when no force is applied to it.

On the other hand, if x_1 and x_2 are not available but the applied forces f_1 and f_2 are, then the interaction force would be computed from the equations of motion. For the above mass-spring system, the equations of motion can be expressed as

$$\begin{aligned} m_1\,\ddot{x}_1(t) &= f_1(t) - F^i(t) \\ m_2\,\ddot{x}_2(t) &= f_2(t) + F^i(t). \end{aligned} \tag{10}$$

By combining the equations in (10), we will have

$$m_1\ m_2\ (\ddot{x}_1 - \ddot{x}_2) = m_2\,f_1 - m_1\,f_2 - (m_1 + m_2)\,F^i. \tag{11}$$

Taking the second derivative of (9) would result in

$$\ddot{F}^i(t) = -k_s\,(\ddot{x}_1(t) - \ddot{x}_2(t)) \tag{12}$$

and plugging (12) into (11) would introduce the interaction force only in terms of the applied forces as

$$C\,\ddot{F}^i(t) + F^i(t) = (1-\alpha)f_1(t) - \alpha f_2(t) \tag{13}$$

where

$$C = \tfrac{-m_1 m_2}{k_s(m_1+m_2)} \text{ and } \alpha = \tfrac{m_1}{m_1+m_2}. \tag{14}$$

Equations (13) and (14) describe the interaction force in the form of a dynamical equation when f_1, f_2 and the system parameters (m_1, m_2, and k_s) are available.

B. Mass-Spring System versus Rigid Body

Modeling objects as a rigid body is a common practice in many problems, due to its simplicity and effectiveness. It is based on the fact that deformation of a solid body in response to small (or moderate) forces is negligible for many materials. This is especially true when the applied forces are within the range of a human–human cooperative manipulation. However, using the rigid body model and ignoring the deformation of the solid body is in part the source of the ambiguity in computation of the interaction force (as discussed in Section III-D).

The mass-spring system generalizes the rigid body model by including object deformation in the model (the spring). For instance, if we replace the spring with a massless rigid rod (or, equivalently, $k_s \to \infty$ in the spring), the mass-spring system becomes one rigid object (with two separated masses). Since the rod is rigid, we have $x_1 = x_2 + L_0$ and, therefore, (11) becomes the same as (6), where α is defined in (14).

Although the generalization introduced by mass-spring system seems promising, unfortunately neither (9) nor (13) can be used to compute the interaction force in a solid body. In the case of (9), although the position variables (x_1 and x_2) are assumed to be available, accurate measurement of these variables is practically infeasible. Furthermore, the value of k_s in a solid body is very large. As a result, any small noise in the measurement of x_1 and x_2 would result in a large error in the computation of F^i.

Similarly, exploiting (13) to compute the interaction force in a solid body is impractical. Here, the large value of k_s would not be a problem and, in fact, it results in a negligible value for C in (14) and, thus, would transform (13) to be the same as (6), as expected. The problem is that any arbitrary values for m_1 and m_2 would work in the mass-spring system and generate a valid model for the solid body. For instance, if $m_1 = m_2$, we get $\alpha = 0.5$ in (14) and it would represent the VL model. Similarly, when $m_1 = 0$ ($\alpha = 0$), the mass-spring system represents the leader/follower model in which f_1 leads the task. In other words, the mass-spring system cannot disambiguate the interaction force model in (6), if (13) is being exploited.

In contrast, we will show that by including the information about the task we can tackle both aforementioned problems. That is, the proposed model for the interaction force is both nonambiguous and robust to the measurement noise. To tackle the ambiguity issue it implicitly takes advantage of the position variables and, to address the noise problem, it exploits the measurements of the applied forces.

C. Task-Aware Interaction Model: A Polynomial Model

Let us assume that the mass-spring system is being manipulated cooperatively, in a cooperative reaching movement task. That is, the subjects move the masses from their initial configurations (x_{i_1} and x_{i_2}) to their final configurations (x_{f_1} and x_{f_2}), following a minimum-jerk trajectory. Since each hand experiences disturbing forces through the spring (the interaction force), the reaching movement is performed inside a force field. As discussed in Section III-C, after enough learning trials, cooperating hands learn to compensate for the force field and return to their original minimum-jerk motion trajectories

$$\begin{aligned} x_1(\tau) &= x_{i_1} + (x_{f_1} - x_{i_1})(6\tau^5 - 15\tau^4 + 10\tau^3) \\ x_2(\tau) &= x_{i_2} + (x_{f_2} - x_{i_2})(6\tau^5 - 15\tau^4 + 10\tau^3) \end{aligned} \tag{15}$$

where $\tau = (t - t_i)/(t_f - t_i)$ and t_i and t_f are the start time and the end time of the cooperative manipulation. As a result, $\Delta x(t) = x_1(t) - x_2(t)$ would also be a minimum-jerk trajectory

$$\Delta x = \delta_i + (\delta_f - \delta_i)(6\tau^5 - 15\tau^4 + 10\tau^3) \tag{16}$$

where $\delta_i = (x_{i_1} - x_{i_2})$ and $\delta_f = (x_{f_1} - x_{f_2})$. Let us rewrite (9) as $F^i(t) = -k_s\,(\Delta x(t) - L_0)$. Similar to the discussions in Section III-C, when $\Delta x(t)$ is a minimum-jerk trajectory, the interaction force would also be a minimum-jerk trajectory

$$F^i(t) = \underset{F}{\operatorname{argmin}} \left(\frac{1}{2} \int_{t_i}^{t_f} \left\| \frac{\mathrm{d}^3 F(t)}{\mathrm{d}t^3} \right\|^2 \mathrm{d}t \right) \tag{17}$$

or, equivalently, the interaction force can be expressed as

$$F^i(t) = \sum_{k=0}^{5} c_k t^k. \tag{18}$$

For a complete model, we need to determine the coefficients, c_k. As explained in Section III-D, when $F_{\text{sum}} = 0$, the value of $F^i = f_1$ is known. According to Section III-B, F_{sum} is associated with a minimum-jerk trajectory (bell-shaped velocity profile). That is, it has exactly one zero crossing point, namely t_m. Therefore, $F_{\text{sum}} = 0$ for $t \leq t_i$, $t = t_m$ and $t \geq t_f$ [see Fig. 5(a)]. This constructs three constraints for the interaction force as

$$\begin{aligned} F^i(t_i) &= f_1(t_i) \\ F^i(t_m) &= f_1(t_m) \\ F^i(t_f) &= f_1(t_f). \end{aligned} \tag{19}$$

Since $F^i(t) = f_1(t)$ for $t \leq t_i$ and $t \geq t_f$, we will have $\dot{F}^i(t_i^-) = \dot{f}_1(t_i^-)$ and $\dot{F}^i(t_f^+) = \dot{f}_1(t_f^+)$. And since both signals are smooth signals

$$\begin{aligned} \dot{F}^i(t_i) &= \dot{f}_1(t_i) \\ \dot{F}^i(t_f) &= \dot{f}_1(t_f). \end{aligned} \tag{20}$$

The five constraints in (19) and (20) determine five coefficients in (18) and the last coefficient is obtained by solving the optimization problem in (17). To calculate the coefficients, let $P_4(t)$ denote the fourth order polynomial that satisfies the constraints in (19) and (20), i.e.,

$$\begin{aligned} P_4(t) &= e_4t^4 + e_3t^3 + e_2t^2 + e_1t + e_0 \\ P_4(t_i) &= f_1(t_i) \quad \dot{P}_4(t_i) = \dot{f}_1(t_i) \\ P_4(t_m) &= f_1(t_m) \quad \dot{P}_4(t_f) = \dot{f}_1(t_f) \\ P_4(t_f) &= f_1(t_f). \end{aligned} \tag{21}$$

Thus, any fifth-order polynomial that satisfies the constraints in (19) and (20) can be expressed as

$$P_5(t, \kappa) = P_4(t) + \kappa(t - t_i)^2(t - t_m)(t - t_f)^2. \tag{22}$$

The interaction force is the fifth-order polynomial that satisfies (17). Thus, by solving (17) for (22), the optimal value of κ is obtained as

$$\kappa^* = \underset{\kappa}{\operatorname{argmin}} \left(\frac{1}{2} \int_{t_i}^{t_f} \left\| \frac{\mathrm{d}^3 P_5(t, \kappa)}{\mathrm{d}t^3} \right\|^2 \mathrm{d}t \right) \tag{23}$$

and the interaction force will be

$$F^i(t) = P_5(t, \kappa^*). \tag{24}$$

Equations (21)–(24) provide the computational model for the interaction force during a dyadic reaching movement.

D. Discussion

To better understand different aspects of the proposed model we provide a list of the characteristics of the model.

1) Assumption: As discussed in Section III-D, to uniquely determine the interaction force one needs to introduce a new constraint to the system. The proposed polynomial model (PM) assumes that the characteristics of the task is given in the form of a computational model for the motion profile (here the minimum-jerk trajectories). As a result of this assumption, the model does not depend on the value of the object's stiffness, k, or the selection of m_1 and m_2.

2) Limitation: The proposed interaction force model is based on the motion model of the cooperative hands. As a result, the level of precision of the model is determined by the precision of the motion model. Since the minimum-jerk model (the motion model we applied) is the nominal model of hand movement, the resulting PM describes the nominal profile of the interaction force. This approximating behavior will be observed in Section VII.

3) Advantage: Unlike the interaction force models discussed in Section III-D, the PM does not require the whole trajectory of applied forces (f_1 and f_2) to obtain the interaction force. More importantly, it can extract the interaction force based on only one of the applied forces, e.g., f_1 in (21). This is particularly important when the robot engages in a cooperative task with a human. We will further exploit this in Section VIII.

4) Disadvantage: The interaction force models discussed in Section III-D can compute the value of F^i at time t only by measuring f_1 and f_2 at the same time, t. The proposed model, however, depends on the values of f_1 in the future times (i.e., at boundary points). This would be a major issue when the robot needs to compute the interaction force in real time. We will further discuss this in Sections VIII and IX.

5) Extension: The mass-spring model relates the interaction force to the deformation of the object. Since elastic deformation appears in many different forms (such as compression, tension, shear, and torsion), one might suggest a more general form of linear relation between the interaction force and the deformation strain. For instance, the model can simply be extended to a more general case by using a mass-spring-damper system. Taking k_d as the damping coefficient, the interaction force would be expressed as $F^i(t) = -k_s\left(x_1(t) - x_2(t) - L_0\right) - k_d\left(\dot{x}_1(t) - \dot{x}_2(t)\right)$. It is easy to see that, if the motion profiles of x_1 and x_2 are available, the interaction force would be obtained as a linear combination of these profiles and their derivatives. In the case of the reaching movement, the resulting interaction force would again be a fifth-order polynomial.

V. Human Study

To be able to evaluate the proposed interaction model we collected human interaction data for bimanual and dyadic object manipulation tasks. In SPB mode, the subjects were asked to grasp an object with both hands and move it horizontally. In dyadic mode, the subjects were grouped into pairs and asked to perform cooperative manipulation. In both cases, the grasps were prehensile and the subjects could apply independent forces and torques to the object.

A. Experimental Setup

We chose a pot as the object to be carried bimanually. To collect the forces applied by the subjects, we used two SI-65-5 ATI Gamma force sensors [40]. The force sensors were placed in between each handle and the pot. The forces are then sampled by a computer through two PCI-6034E NI data acquisition boards [41] at the frequency of 1 KHz. The acquired data is then

Fig. 7. Experimental setup. The force sensors are installed between the handles and the container. The IMU is interfaced with a Arduino board and placed in a box that is glued to the inside bottom of the pot. The sampled data is collected by a GUI in MATLAB.

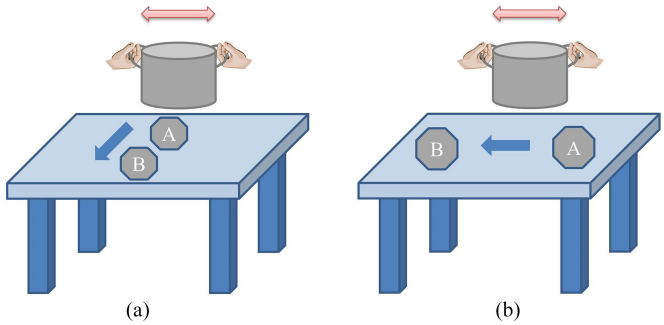

Fig. 8. (a) Type 1 and (b) type 2 motions. In SPB manipulation, the person stands behind the table and grabs the handles. In dyadic manipulation, the subjects stand on the opposite sides of the table and grab the handles. The blue arrow on the table shows the motion direction and the red double arrow is the grasp force.

transformed to the earth reference frame. This requires the orientation of the pot to be measured. We used a 9DOF-Sensor-Stick SparkFun IMU to measure the pot's orientation and acceleration [42]. The sampling frequency for the IMU is set to 100 Hz. The IMU is interfaced with the computer through an Arduino Mega microcontroller board [43]. All data collection is managed through a MATLAB GUI that we have developed. Fig. 7 shows the experimental setup and its components. To eliminate the high-frequency noise, a low-pass FIR smoothing filter with the cutoff frequency of 12.5 Hz is applied to the signals.

B. Experimental Procedure

Each trial of the experiment consisted of three subtasks; lifting the pot from the table at the start point (point A), moving the pot horizontally toward the destination point (point B), and putting the pot down on the table at the end point. Studies have shown that gravity plays a significant role in single-arm vertical reaching movements [44], [45]. Therefore, in this study we focus on the horizontal movements and discard the first and last subtasks in each trial. We will consider these vertical movements in our future works.

To improve the synchronization between the subjects in dyadic mode, a beep was played at fixed points in time by the software and the subjects were told to execute each subtask right after hearing the beep. Therefore, the start time of the motion was known for both subjects. The start point and the end point were marked to provide x_i and x_f. The configurations of the start points and the end points were designed in such a way that we have two types of horizontal motions. In type 1 motions, the direction of the motion is perpendicular to the line connecting the handles. Therefore, the grasp force has small components in the motion direction. In type 2 motions, the direction of the motion is parallel with the line connecting the handles and grasp force has dominant components in this direction (see Fig. 8). In addition, the distances between the start points and the end points were selected such that both short-range and long-range motions were included. In the short-range motions, the horizontal distance between the start point and the end point was 28 cm and in the long-range motions it was 83 cm.

C. Data Collection

According to our IRB protocol, we were allowed to recruit participants by using flyers and emails. The approved flyers were posted in buildings around the University of Illinois at Chicago (UIC) campus. In addition, a recruitment email was sent to the graduate student list server at UIC. As a result, the participants belonged to the body of the UIC students, staff, and their acquaintances. Among all volunteers, we recruited 22 adult subjects (12 men and 10 women), ranging in age from 19 to 35.

The data collection was performed in the Robotics Laboratory at the UIC. The experiments were scheduled over the course of ten days, according to the participant's availability. The subjects were randomly paired and assigned to a specific session. In each session, after briefing the participants about the project's goals, benefits and risks, they signed consent forms. Then the task was explained and demonstrated to them, including different modes (bimanual versus dyadic) and different tasks (motion types and motion ranges).

Next, each subject was given enough familiarization trials (as many as they needed). Then, he/she performed three trials in the SPB scenario, including a short-range type 1 motion, a short-range type 2 motion, and a long-range type 2 motion. The long-range type 1 motion was skipped, because it was not within the range of human-arm reachable space. Then, the subjects were grouped into pairs (dyadic mode). Subjects in each pair stood on the opposite long-sides of the table and performed three more trials. The motion direction in all trials is along the length of the table. To generate different motion types, the pot was yawed to be parallel with or orthogonal to the motion direction. In all of the trials no repeated measurements were collected. Each session took less than an hour and each participant was paid upon completion of all of the tasks.

D. Data Analysis

We collected 33 trials (11×3) in dyadic mode and 63 trials (21×3) in bimanual mode (one of the participants refused to complete the task in this mode). Then, the collected data were analyzed to identify the measurement errors. The errors were mainly due to the hysteresis error that the sensors exhibited randomly. We examined the value of F_{sum} to identify the measurement error. For instance, if the pot was not moving (ac-

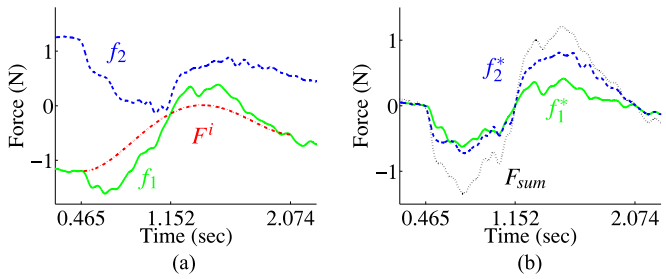

Fig. 9. Example of calculating interaction force and effective forces. The solid green signal is f_1 (f_1^*), the dashed blue signal is f_2 (f_2^*), the dotted black signal is F_{sum}, and the dash-dotted red signal is F^i. In this example, $t_i = 0.46\ s$, $t_m = 1.15\ s$, and $t_f = 2.07\ s$. (a) Applied forces and (b) effective forces.

cording to the IMU readings), a constant large value in F_{sum} would indicate the presence of the hysteresis error. As a result, two trials in dyadic mode and five trials in bimanual were marked as corrupted signals.

After the corrupted trails were excluded, the data was processed to compute the interaction force, F^i. That is, first the PM in (21)–(24) was applied to the collected data (f_1 and f_2). Then, the effective forces, f_1^* and f_2^*, were obtained from (4). Fig. 9 demonstrates the result of this procedure for a single sample trial. The collected applied forces and computed interaction force are shown in panel (a) and the effective forces along with F_{sum} are presented in panel (b). It is worth mentioning that the optimization problem in (23) was solved numerically, using the optimization toolbox in MATLAB. The above data processing procedure was performed again, using the VL model and ME model. Here, F^i was computed using (7) and (8), respectively.

VI. Evaluation of the Proposed Model

In this section, we study the characteristics of the PM in comparison with the VL model and the ME model. To explore different features of an interaction force signal, we use five different quantitative metrics (given in the Appendix). Different metrics measure different features of a signal, such as average, energy, and variation rate. Furthermore, since computing either interaction force (F^i), effective forces (f_1^* and f_2^*), or α gives the other two [refer to (4) and (5)], different metrics use different variables to explore the features space more broadly [see (33)–(37)]. For more details on the metrics and their properties, refer to [23].

Recall that each subject performed three trials in each session. In addition, recall that for each trial the interaction force was computed in three different ways (three models). Since for each computed force we measure five features, a total of 45 observations are collected per subject. On the other hand, we had 32 subjects (21 participants and 11 pairs) and, therefore, the full list of observations would have 32×45 entries. However, to deal with the seven missing data (corrupted measurements), we performed a listwise deletion and, thus, the number of subjects became 16 participants and nine pairs. We grouped the subjects according to the cooperation mode. That is, 16 participants were placed in the bimanual group and nine pairs were placed in the dyadic group.

We are interested in studying the effects of both the interaction model and the cooperation mode on the properties of the interaction force. Since the models are based on different assumptions, it is expected that their interaction force signals, $F^i(t)$, show different properties. In addition, since only one brain controls both hands in the bimanual mode (versus two brains in the dyadic mode), it is expected that the properties of F^i are different between the two modes. To study these hypotheses, we set up a repeated measures ANOVA test. The between-subjects factor (mode) has two levels, bimanual and dyadic. The within-subjects factors are model (three levels), task (three levels), and feature (five levels). The test includes a total of 45 repeated measurements for each of the 25 subjects.

Mauchly's test of sphericity showed that the assumption of sphericity had been violated ($\chi^2(989) > 10000$, $p < .0001$) and, therefore, a Greenhouse–Geisser correction ($\hat{\varepsilon} = 0.086578$) was applied. The repeated measures ANOVA with a Greenhouse–Geisser correction determined that a statistically significant interaction exists between the cooperation mode and the interaction model [$F(0.173, 3.983) = 8.666$, $p < 0.0019$]. The significance level was $\alpha = 5\%$ in this test. No any other statistically significant interaction was observed ($p > 0.05$ for all). No significant main effect was observed, except for the cooperation mode [$F(0.087, 1.991) = 8.406$, $p < 0.0081$], which was shadowed by its significant interaction with the interaction model. To further study the role of these interacting factors, simple main effect analysis was performed and a pairwise multiple comparisons posthoc test with the Bonferroni correction was employed.

To test the first hypothesis, we took the cooperation mode as the moderator variable. We observed significant differences between the means of the PM, VL, and ME, when the cooperation mode was bimanual ($p < 0.0001$ for all). In the case of the dyadic cooperation, while significant differences between the mean of VL and the means of the PM and ME were observed ($p < 0.0001$ for both), no significant difference was observed between the means of PM and ME ($p > 0.88$). The test results indicate that, regardless of the cooperation mode, VL model introduces a statistically significantly different F^i than PM and ME. Furthermore, PM and ME introduce statistically significantly different F^i in bimanual mode. However, not enough evidence existed to draw the same conclusion in the dyadic mode. This is a fairly expected conclusion, considering the difference between the assumptions taken by different models.

For the second hypothesis, the interaction model was taken as the moderator variable. We observed a significant difference between the means of bimanual and dyadic groups in the PM model ($p < 0.0001$), while no significant difference was observed in the case of VL and ME models ($p > 0.76$). These results indicate that the interaction forces (F^i) appearing in the bimanual mode are statistically significantly different from the ones appearing in the dyadic mode, when the PM model is employed. For the other two models there is not enough evidence to draw similar conclusions. This observation does not strongly support our hypothesis and the test failed to reject

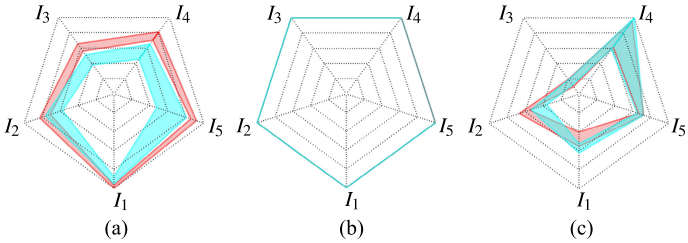

Fig. 10. Radar charts of the 95% confidence intervals of the means of all five metrics obtained for different models in different modes. The red and cyan charts represent the statistics for the bimanual and dyadic modes, respectively. (a) Polynomial. (b) VL. (c) ME.

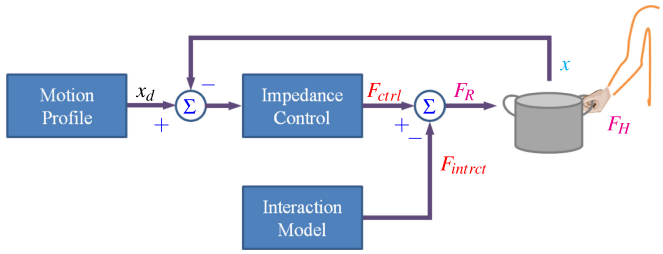

Fig. 11. Control diagram. The interaction force is introduced in a feed-forward manner.

the null hypothesis when VL or ME is employed. To better understand this observation, we have visualized it in Fig. 10.

Panels (a), (b), and (c) in this figure show radar charts for PM, VL, and ME models, respectively. In all charts, the red patches are associated with the bimanual mode and the cyan patches present statistics for the dyadic mode. The depicted statistics are the 95% confidence intervals of the means for the measured features. For example, the red interval on I_1 axis in panel (a) shows the 95% confidence intervals of the means of the I_1 samples, when only PM and bimanual levels are considered in model and mode factors, respectively. Recall that all of the metrics are bounded between zero and one. Thus, the charts axes are all between zero and one, with zeros at the center of the chart.

As illustrated in Fig. 10(a), when the PM model is employed, bimanual and dyadic modes are statistically significantly different in all metrics (except I_2). However, when the VL model is used, no discrepancy exists between the metrics [see Fig. 10(b)]. That is due to the fact that $f_1^* = f_2^*$ and $\alpha = 0.5$ when the VL model is employed [see (7)]. Plugging these values in (33)–(37) would give a constant value of one for all metrics. Finally, Fig. 10(c) shows that the confidence intervals in bimanual and dyadic modes overlap (except for I_2) when ME model is used.

The test results suggest an interesting conclusion: PM would effectively capture the difference between the bimanual mode and the dyadic mode, VL would always fail to do so, and not enough evidence existed that ME can do the same. In other words, considering the existing sample population, the proposed PM captures the critical information of the interaction better than the other two models. However, it is important to note that we based our study on a specific set of metrics. While we did our best to explore different aspects of the interaction force, it is possible that this set has not captured all the important dimensions of the feature space. As a result, the aforementioned conclusion is under the influence of the metrics defined in the Appendix.

VII. Robot Controller Based on the Interaction Force

In this section, we test our hypothesis that the robot performs more efficiently when it is provided with the interaction force. We introduce a controller scheme that exploits the interaction force to generate robot's applied force. The efficiency of the robot is evaluated using a measure of position error.

A. Simulation Setup

To measure the performance of these models, we propose the following scenario. First, the applied forces during performing a dyadic (or bimanual) object manipulation task are assumed to be available (our recorded data). Next, we calculate the interaction forces based on all three models (offline). Then, we replace one human (or one hand) with a robot and provide the robot's controller with the computed interaction force. Finally, we compare the performance of the human–robot cooperative manipulation with respect to the human–human dyadic (or bimanual) manipulation, in terms of root-mean-squared error (RMSE).

To make sure that the measured error reflects the difference between the models (and is not dominated by another factor), we take the following steps. We assume that the robot has a full knowledge about the task; that is, x_i, x_f, t_i, t_f and the object's mass, M, are all known to the controller. We chose the impedance control over position control to make the controller responsive to the interaction force. We also assumed that the robot can be controlled perfectly so that the commanded force appears at the robot's end effector identically and immediately.

Since the controller is based on the *offline computed* interaction force, it is not causal. Particularly, it cannot be utilized for a real robot that is interacting with a human in an online fashion. Throughout this section, the term "robot" refers to a virtual agent (or the controller itself), rather than an actual robot. In Section VIII we introduce a causal controller to be implemented on a real robot. The controller exploits an online estimate of the interaction force instead of the offline computed one.

Fig. 11 shows the block diagram for the offline controller. The contribution of the robot to the manipulation task is shaped by the motion profile block. It generates the desired object trajectory x_d that is a minimum-jerk trajectory in our case (see Section III-B). The impedance control block generates the controller force F_{ctrl}, which guarantees a stable tracking of this desired trajectory. Thus, F_{ctrl} is the contribution of the robot to the cooperative task. On the other hand, the interaction model block provides the interaction force F_{intrct}. Thus, the robot applied force, F_R, is then construed as

$$F_R = F_{\text{ctrl}} - F_{\text{intrct}}. \tag{25}$$

Based on (4), human–human cooperation and human–robot cooperation can be formulated as

$$\begin{aligned} F_H &= F_H^* + F^i & F_H &= F_H^* + F_{\text{intrct}} \\ F_h &= F_h^* - F^i & F_R &= F_{ctrl} - F_{\text{intrct}} \end{aligned} \tag{26}$$

where F_H (F_H^*) and F_h (F_h^*) are the human applied (effective) forces. More specifically, F_h is the force that we intend to replace with the robot force (F_R) and F_H is the force that the robot wants to cooperate with.

If we take the calculated human interaction force as the human–robot interaction force, $F_{\text{intrct}} = F^i$, and if the robot uses the human–human motion trajectory, x_{Hh}, as the desired trajectory, $x_d = x_{\text{Hh}}$, the robot's effective force will follow the other human's effective force, $F_{\text{ctrl}} = F_h^*$. Here, we assume that the actual motion trajectory of a human–human dyadic manipulation (x_{Hh}) is not available to the robot. Thus, the robot uses the minimum-jerk model as an estimate of the human–human motion trajectory and, therefore, F_{ctrl} approximates F_h^*. The impedance control that provides robot's effective force is

$$F_{\text{ctrl}} = M\,\ddot{x}_d + K_d(\dot{x}_d - \dot{x}) + K_s(x_d - x) - \frac{1}{2}M\,\bar{g} \quad (27)$$

where M is the object's mass, $K_d = 5M$, and $K_s = 6M$. The values of K_d and K_s are selected in such a way that the poles of the closed-loop system are small ($p_1 = -2$ and $p_2 = -3$). It allows the robot to interact with the human, while keeping the tracking error small. The last term in (27) compensates half of the weight of the object, assuming that the human compensates the other half. Apply (25), (26), and (27) to the object's equation of motion, $F_R + F_H + M\bar{g} = M\,\ddot{x}$. Therefore

$$M\,\ddot{e} + K_d\,\dot{e} + K_s\,e = \tilde{F}_H \quad (28)$$

where $e = x - x_d$ and $\tilde{F}_H$ are the human's gravity-compensated effective force, $F_H^* = \tilde{F}_H - \frac{1}{2}M\,\bar{g}$. Equation (28) shows that the controller is BIBO stable and the tracking error is a function of human effective force.

B. Simulation Results

For each trial of the human study, we consider the applied forces to the pot (f_1 and f_2) and calculate the interaction forces (F^i) based on three models: VL, ME, and PM. These interaction forces are used in the interaction model block in the robot controller in Fig. 11. That is, we apply $F_{\text{intrct}} = F^i$ for the above three models. To study the necessity of including the interaction force in the robot controller, we consider the case in which $F_{\text{intrct}} = 0$. We will refer to this model as the zero-interaction-force (ZF) model.

Fig. 12 illustrates an example of the performance of the robot for different interaction models. The motion trajectory of the human–human cooperation (x_{Hh}) is considered to be the baseline for comparing the performance of the models. In Fig. 12(a), this trajectory is marked with small circles (Hh). The motion trajectories of VL, ME, and PM closely follow the human–human trajectory. However, the zero-interaction-force (ZF) trajectory cannot follow x_{Hh}. This means that although the impedance controller attempts to contribute to the task and move the pot along the desired trajectory, due to the lack of a good model for the interaction force robot forces conflicts with human's and the whole task fails. This is more evident in Fig. 12(b), where the difference between the x_{Hh} and the human–robot motion trajectories (x_{HR}) with different interaction models are illustrated. While the position error for VL, ME, and PM are very similar

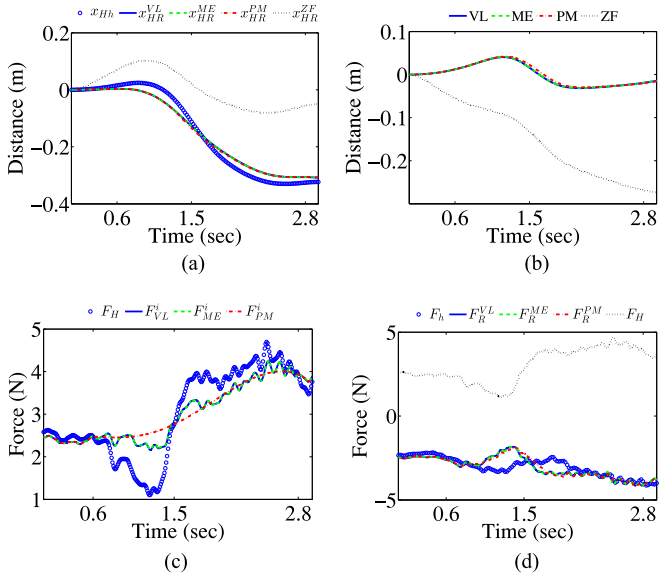

Fig. 12. Example of the performance of the robot, using different interaction models. (a) Motion trajectory of human–human cooperation (x_{Hh}) is compared with human–robot motion trajectory (x_{HR}) using the VL, ME, PM, and ZF models. (b) Robot's performance in terms of the position error: $d = x_{\text{Hh}} - x_{\text{HR}}$. (c) Interaction force (F^i) compared with the human force (F_H). (d) Robot force (F_R) compared with both humans forces. F_h is the human force that we intend to replace with the robot force and F_H is the human force that the robot wants to cooperate with. (a) Motion trajectories *x*Hh and *x*Hr, (b) position error *x*Hh-*x*HR, (c) interaction forces and FH, and (d) robot forces F_h and F_H.

and less than 5 cm, the position error for ZF increases to 28 cm. We will use this error signal to statistically compare these models with each other in the next section.

Fig. 12(c) shows the human applied force (F_H) and the interaction forces generated by different models. As illustrated here, VL and ME models generate very similar interaction forces and PM generates a low-order approximation of those interaction forces. These interaction forces shape the robot's applied force (F_R). As it appears in Fig. 12(d), the robot's force (F_R) follows the replaced human force (F_h) in all models, as expected. However, there exist a distinct difference between F_R and F_h, due to the difference between robot's desired trajectory and human's original trajectory ($x_d \neq x_{\text{Hh}}$).

C. Statistical Evaluation

We are interested in studying the effect of different interaction force models (PM, VL, ME, and ZF) on the performance of the proposed controller. Comparing the performance requires an evaluation measure to be introduced. Let $d(t)$ be the difference between the human–human motion trajectory and the human–robot motion trajectory, $d(t) = x_{\text{Hh}} - x_{\text{HR}}$. We used the root mean square of $d(t)$ as the evaluation measure

$$\text{RMSE} = \sqrt{\frac{1}{t_f - t_i}\int_{t_i}^{t_f} \|d(t)\|^2\,\text{d}t}. \quad (29)$$

The measure evaluates the performance of the controller in terms of the average position error, given the specific interaction model used. We use the sample population of the RMSE to sta-

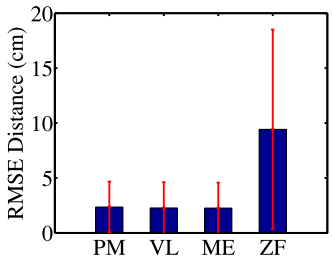

Fig. 13. Average performance of the robot, using different interaction models: VL model, ME model, PM, and ZF model.

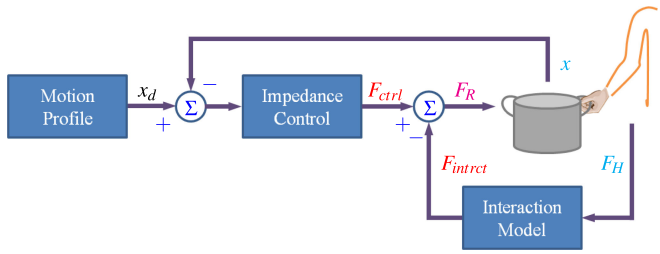

Fig. 14. Sketch of the control diagram. The position of the pot and the human applied force are measured and sent to the robot controller.

tistically compare the effect of the interaction models. The mean and standard deviation of the samples for different models are PM : (2.36 ± 2.31), VL : (2.27 ± 2.35), ME : (2.25 ± 2.32), and ZF : (9.43 ± 9.09) all in cm. Fig. 13 shows the mean and standard deviation of RMSE measure when different interaction models are employed. As illustrated in the figure, the ZF model generates larger mean error than the other three models and the average error introduced by PM is not very different from VL's error or ME's error.

In Section VI we discussed that the properties of the interaction force are different among different models. Therefore, it is expected that the performance of the controller would also be different between the models. To evaluate this hypothesis, we set up another repeated measures ANOVA test. The ANOVA model is very similar to the one described in Section VI. The between-subjects factor "mode" and the within-subjects factor "task" are the same as before, but the within-subjects factor "model" has four levels, PM, VL, ME, and ZF. The test includes a total of 12 (3×4) repeated measurements for each of the 25 subjects.

Mauchly's test of sphericity showed that the assumption of sphericity had been violated ($\chi^2(65) = 894.05$, $p < .0001$) and, therefore, a Greenhouse–Geisser correction ($\hat{\varepsilon} = 0.23046$) was applied. The repeated measures ANOVA with a Greenhouse–Geisser correction determined that the mean RMSE differed statistically significantly among different models [$F(0.6914, 15.9017) = 25.576$, $p < 0.0001$]. Furthermore, no statistically significant interaction was observed between "model" and other factors ($p > 0.15$ for all). The significance level was $\alpha = 5\%$ in the test. A pairwise multiple comparisons post-hoc test with the Bonferroni correction was performed. We observed that the mean RMSE error is statistically significantly higher when ZF is used ($p < 0.0003$ for all three pairwise tests). Moreover, no statistically significant difference was observed between the means of PM, VL, and ME ($p > 0.82$ for all tests). The test results suggest the following two conclusions.

First, informing the controller about the properties of the interaction force would significantly increase its performance. This conclusion, which is not surprising, would support the exploitation of the interaction force models in designing an online controller (see the next section).

Second, no enough evidence existed to suggest that the performances of different controllers (with PM, VL, and ME models) are statistically significantly different from each other. This is a surprising conclusion, considering our discussion on the differences between the properties of the interaction force among these models (see Section VI). We speculate that the impedance controller block would have partially compensated for the differences between the interaction models and resulted in this observation.

VIII. Human–Robot Cooperation Strategy

In designing the control scheme in the previous section, we discussed that taking the human–robot interaction force equal to the calculated human interaction force ($F_{\text{intrct}} = F^i$) leads to a human–robot motion trajectory that closely follows the human–human motion trajectory. Thus, we assumed that the interaction force between humans was fully known (calculated offline) and the interaction model block in Fig. 11 was designed in a feed-forward manner.

In the case of a real-time human–robot interaction, no human–human interaction exists as a reference and, therefore, the controller needs to calculate the interaction force only based on the human's applied force F_H. Fig. 14 shows the real-time robot controller block diagram, in which the interaction model block measures the human force F_H and estimates the interaction force F_{intrct}. The design of the rest of the controller is exactly the same as discussed in the previous section. In the next section, we introduce an algorithm that estimates F_{intrct}, by predicting F_H and utilizing the PM.

A. Estimating the Interaction Force

We showed that the PM demonstrates a satisfactory performance in an offline controller. We also discussed that while other interaction models require both human forces (F_H and F_h) to calculate the interaction force (F^i), PM provides a good approximation for F^i, using only one force (F_H). Moreover, the model requires only five boundary values to identify the interaction force. As a result, PM is a good candidate for estimating F^i. According to the PM model, (21)–(24), the interaction force requires the value of F_H to be known at times t_i, t_m, and t_f. However, when the robot is calculating $F_{\text{intrct}}(t)$ for times $t < t_m$ (or $t < t_f$), the future human force, $F_H(t_m)$ [or $F_H(t_f)$], is not available yet. Therefore, in order to use PM model as an estimator of the interaction force, either the boundary values or the whole future human force need to be predicted.

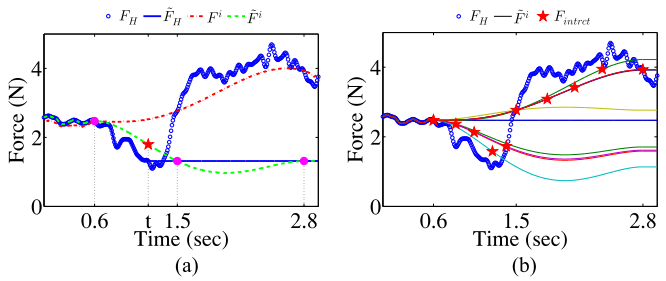

Fig. 15. Example of estimating F_{intrct} at time t. Since neither the human force (F_H) nor the PM interaction force (F^i) is available to the robot after time t, the controller predicts them ($\tilde{F}_H$ and $\tilde{F}^i$, respectively). (a) The predicted boundary conditions are marked with magenta dots and the estimated interaction force at time t [$F_{\text{intrct}}(t)$] is marked by a red star. (b) As time increases, the simulated robot's estimation of F_{intrct} evolves (intermediate curves) and $\tilde{F}^i$ approaches F^i. (a) Estimating F_{intrct} *(t)*. (b) Evolution of $\tilde{F}_i$.

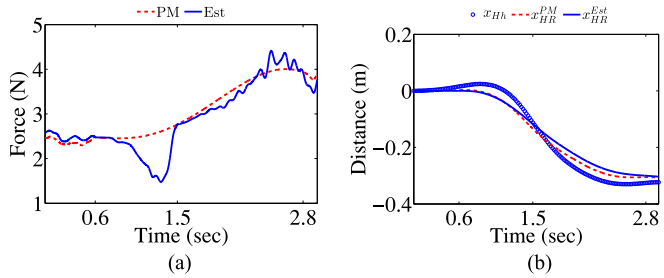

Fig. 16. Example of the performance of the robot using the cooperation strategy. (a) Simulated online interaction force estimation (Est) is compared with the offline calculated PM. (b) Motion trajectory of human-human cooperation (x_{Hh}) is compared with human–robot motion trajectory (x_{HR}) using PM and estimated interaction force (Est). (a) Interaction Forces. (b) Motion trajectories.

Let us define the predicted human force $\tilde{F}_H$ as

$$\tilde{F}_H(\tau, t) = \begin{cases} F_H(\tau) & \tau \le t \\ F_H(t) & \tau > t \end{cases} \tag{30}$$

where τ is the time variable ($0 \le \tau < \infty$) and t represents the current time. The predictor suggests that human's applied force in the future remains constant and equal to the current force value. While it is the simplest prediction of the future values of F_H, it is motivated by the minimum-jerk constraint. It is easy to see that (1) minimizes $||\dot{F}_H(t)||^2$ and, thus, $\dot{F}_H(t) = 0$ (or $F_H(t) = Const.$) is the optimal solution. However, this justification is based on the assumption that the manipulation task is mainly performed by the robot and the human only provides a constant interaction force (e.g., grasp force).

If we plug (30) into (21)–(24), the interaction force that is predicted at time t for the whole task ($t_i \le \tau \le t_f$) would be obtained as

$$\tilde{F}^i(\tau, t) = \text{PolynomialModel}\left(\tilde{F}_H(\tau, t)\right) \tag{31}$$

which is a fifth-order polynomial, satisfying the predicted boundary values. As a result, the estimated interaction force at time t would be

$$F_{\text{intrct}}(t) = \tilde{F}^i(\tau = t, t). \tag{32}$$

Fig. 15(a) shows the above procedure for the same human force (F_H) as we studied in the previous section. The prediction of human force for $t \ge 1.14$, $\tilde{F}_H$ is shown with a blue solid line and the boundary values at $t_m = 1.5$ and $t_f = 2.8$ are marked as magenta dots. The PM model is employed and the predicted interaction force, $\tilde{F}^i(\tau, t)$, is calculated and shown with the green dashed line. The estimated interaction force at time t, $F_{\text{intrct}}(t)$, is obtained and marked by a red star. Note that the estimated value is very different from the offline calculated interaction force, $F^i(t)$ (red dashed-dotted line). However, as time increases, $\tilde{F}^i$ approaches F^i and the estimated value $F_{\text{intrct}}(t)$ gets closer to $F^i(t)$. Fig. 15(b) shows the evolution of $\tilde{F}^i$ with several intermediate curves. As $\tilde{F}^i$ curves approach F^i, the estimated interaction force values (red stars) get closer to the offline calculated interaction force.

Fig. 16 compares the performance of the online and the offline controllers. Fig. 16(a) compares the estimated interaction force with the offline-calculated one. Note that the estimated force is the same as the red star marks in Fig. 15(b). The motion trajectories of both online and offline controllers are also compared with the human–human motion trajectory. As illustrated in Fig. 16(b), while we use a simple prediction for human force, the estimated interaction force results in a high performance. However, it does not mean that the predicted human force $\tilde{F}_H$ is a good representative of F_H. It only provides the required information about the boundary values.

Remark 1: In addition to the simplicity and high performance, the proposed estimator possesses the following interesting features:

1) The proposed estimator guarantees the smoothness of the estimated interaction force (subject to the smoothness of the human applied force).
2) The boundary conditions are always satisfied: $F_{\text{intrct}}(t_i) = F_H(t_i)$, $F_{\text{intrct}}(t_m) = F_H(t_m)$, and $F_{\text{intrct}}(t_f) = F_H(t_f)$. Therefore, as $t \to t_f$, we have $\tilde{F}^i(\tau, t) \to F^i(\tau)$.

B. Statistical Evaluation

We are implementing the control strategy on a four-DOF Barrett's WAM robotic arm [46] as our future work. Thus, to make sure that the dynamics of the robot and the object will be modeled precisely during our simulations, we used MathWorks' SimMechanics simulation environment and the STL files for the WAM arm (provided by the manufacturer). To be faithful to the experimental setup, we used a pot as to be the manipulated object with the same kinematic and dynamic properties as the actual pot. Fig. 17 shows the simulation setup for the controller evaluation.

Since the robot has only four DOF, we use a passive ball joint between the robot and the pot. Therefore, the orientation of the pot is controlled only by the human. In the simulation, we used the orientation data that was recorded from IMU during the experiment to reproduce the correct orientation of the pot.

Similar to the implementation in Section VII-A, we assumed that the robot has a full knowledge about the task. In addition, we assumed that no friction or nonlinearity exists in the robot and

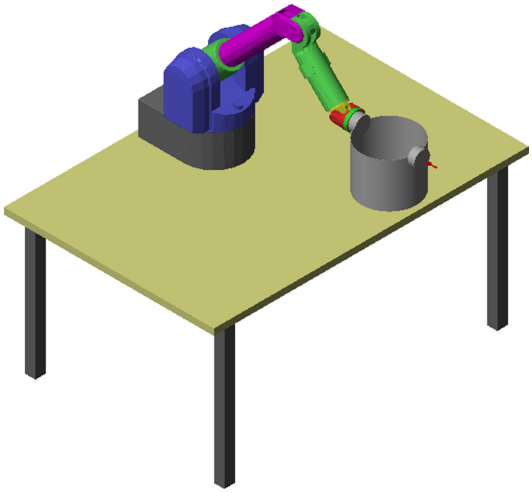

Fig. 17. We used a four-DOF WAM arm to evaluate our proposed model and test the robot's controller with the actual humans' signals. The red arrow at the free pot handle represents the human applied force.

that it can be controlled perfectly. We implemented the control diagram in Fig. 14 as the robot controller. The desired trajectory x_d is a minimum-jerk trajectory given by (1). The impedance controller follows (27) and the interaction model estimator is described by (30)–(32). To measure the performance of the online controller, the same scenario as in Section VII-A was followed. To evaluate the performance of the online controller, we took the same approach as we discussed in Section VII-C and utilized the same RMSE measure as in (29). Let "Est" refer to the population of RMSE error samples obtained in this scenario. The mean and standard deviation for Est is (2.43 ± 2.37) cm.

Consider Fig. 16(a); while the estimated interaction force F_{intrct} follows the offline-calculated interaction force F^i, there is a considerable difference between them. In addition, recall the poor performance of the controller when no information about the interaction force is available (discussed in Section VII-C). These observations suggest that the performance of the proposed online controller (using the estimator) would be higher than the ZF model, but probably lower than the PM model. To study this hypothesis, we set up another repeated measures ANOVA test. This ANOVA model has the same factors as the one described in Section VII-C except that the within-subjects factor model has five levels (PM, VL, ME, ZF, and Est) here. The test includes a total of 15 (3×5) repeated measurements for each of the 25 subjects.

Mauchly's test of sphericity showed that the assumption of sphericity had been violated ($\chi^2(104) = 1154$, $p < .0001$) and, therefore, a Greenhouse–Geisser correction ($\hat{\varepsilon} = 0.18648$) was applied. The repeated measures ANOVA with a Greenhouse–Geisser correction determined that the mean RMSE differed statistically significantly among different models [$F(0.7459, 17.1562) = 25.497$, $p < 0.0001$]. Furthermore, no statistically significant interaction was observed between the model and other factors ($p > 0.15$ for all). The significance level was $\alpha = 5\%$ in the test. A pairwise multiple comparisons post-hoc test with the Bonferroni correction was performed. We observed that the mean RMSE error is statistically significantly higher when ZF is used ($p < 0.0005$ for all four pairwise tests). Moreover, no statistically significant difference was observed between the means of PM, VL, ME, and Est ($p > 0.61$ for all six tests).

The test results supports our hypothesis in part. That is, the estimator provides enough information about the interaction that the performance of the controller is statistically significantly higher than ZF model. However, no enough evidence existed to suggest that the performances of online controller (Est) is statistically significantly different from offline controllers (with PM, VL, and ME models). These observations suggest that the human–robot cooperation strategy, proposed by the control scheme in Fig. 14, would be a promising candidate for an effective human–robot cooperative manipulation.

C. Discussion

A key limitation of our simulation approach is that the human applied forces had been recorded during the experiment (between humans) and then were played back during simulations (between human and robot). In other words, we did not model the possible changes in the human applied forces due to the robot's actions in our simulations. In fact, we do not have access to a model that fully describes how human behavior varies in response to an external force. As a result, although the simulation results are very encouraging, unsatisfactory interactions may appear during an actual human–robot interaction.

On the other hand, human perception is usually noisy. Therefore, if the robot's applied forces are in the range that the human expects to perceive, it may not influence the human's behavior. Based on the promising results observed in the simulations, we speculate that the online controller will demonstrate a satisfactory performance in practice as well, but to test this hypothesis one needs to set up a new study and test the online controller in a real human–robot experiment. We explain our future work on this matter in the next Section.

IX. Conclusion and Future Works

In this paper we studied the properties of the exchanged force during a dyadic manipulation task. Using the existing theories of human-hand motions, we proposed a PM for the interaction force in a dyadic reaching movement. To validate our model, we conducted a study with 22 subjects. We compared our model with the VL model and ME model in a 5-D feature space and observed the following things. First, the features of the interaction force are statistically significantly different among the models (except between ME and PM in the dyadic mode). Second, while the PM model would effectively capture the difference between the bimanual and dyadic types of collaboration, VL would always fail to do so and not enough evidence existed that ME can do the same.

Next, we embedded the models in an impedance controller and observed the following results. First, the performance of the controller is statistically significantly higher when the interaction force information is provided to the robot (using any model). Second, no enough evidence existed to suggest that the

performances of different controllers (using all models) are statistically significantly different from each other. We concluded that the proposed model captures the critical information conveyed by the interaction force and provides a low-order approximation for it.

To be able to embed the interaction model in an online controller, the model should be causal and should depend only on the human's measured force. By applying the PM on a prediction of human's future forces, we proposed a causal estimator for the interaction force. We showed that the proposed online controller demonstrates a high performance similar to the offline controllers. That is, not enough evidence existed to suggest that their performances are statistically significantly different. Considering 1) the difference between the estimated and the offline-calculated versions of the interaction force and 2) the poor performance of the controller when no interaction force is provided, we concluded that these encouraging results are due to an interplay between the impedance controller and the interaction model. Thus, we speculated that the online controller would be a promising candidate for an effective human–robot cooperative interaction.

All these promising results have been achieved by applying our knowledge of the task to the control problem. For instance, in our case a computational model for the reaching movement is the core of the proposed controller and estimator. While the task information is shared between the cooperating agents, the parameters of the task might not be. For instance, in a dyadic reaching movement, the initial and final configurations (x_i and x_f) are known for both persons, but they may have different preferred speeds (different t_m and t_f). The learning trials are used to let the agents negotiate on these parameters and come to an agreement about the value of these parameters.

Similarly, the robot needs to learn about the human's preferred values for these parameters. In the case of the reaching movement, the robot needs to know the values of t_i, t_m, and t_f for both generating its desired trajectory (x_d) and estimating the interaction force (see Sections VII-A and VIII-A). In the simulations, we used the recorded data to provide these information to the robot. For our future experiment with the WAM arm, we will first let the human performs the task in the SPB mode. Next, the parameters will be obtained using the person's recorded data. Then, the human and the robot will be given few learning trials to adapt to each other. We speculate that the human's satisfaction in this scenario would be as high as when the task is performed with a human partner. Designing an adaptation algorithm for these parameters or an online learning mechanism, using Bayesian approach for instance, would be an interesting extension to this study.

APPENDIX

To be able to quantitatively assess different aspects of the signals appearing in the interaction, we employ five performance metrics as follows. A complete list of related indexes and their interpretations (according to the associated human assessment) has been presented in [23]. The variables used in defining the following indexes (such as α, F_{sum}, and effective forces f_1^* and f_2^*) are defined in Section III-D. In addition, t_i and t_f are the start time and the end time of the cooperative manipulation.

Average Wasted Effort: The index measures the level of disagreement between the applied forces. It is defined as

$$I_1 = \frac{1}{t_f - t_i} \int_{t_i}^{t_f} M_1(t)\, \mathrm{d}t \tag{33}$$

where

$$M_1(t) = \frac{\|F_{\text{sum}}(t)\|}{\|f_1^*(t)\| + \|f_2^*(t)\|}.$$

Since $F_{\text{sum}} = f_1^* + f_2^*$, a higher value of the index indicates less average wasted efforts. The index is suitably bounded between zero and one ($0 \leq I_1 \leq 1$), see [23].

Energy-Wise Similarity: The index measures the similarity between the effective forces in terms of the signal-energy. It is defined as

$$I_2 = 1 - \left| \frac{N_1 - N_2}{N_{\text{sum}}} \right| \tag{34}$$

where

$$\begin{cases} N_1 = \int_{t_i}^{t_f} \|f_1^*(t)\|\, \mathrm{d}t \\ N_2 = \int_{t_i}^{t_f} \|f_2^*(t)\|\, \mathrm{d}t \\ N_{\text{sum}} = \int_{t_i}^{t_f} \|F_{\text{sum}}(t)\|\, \mathrm{d}t. \end{cases}$$

A higher value of the index indicates smaller differences between the contributions of the subjects (in terms of signal-energy of the forces). The index is suitably bounded between zero and one ($0 \leq I_2 \leq 1$), see [23].

Time-Wise Similarity: The index measures the similarity between the effective forces at each point in time. It is defined as

$$I_3 = \frac{1}{t_f - t_i} \int_{t_i}^{t_f} M_3(t)\, \mathrm{d}t \tag{35}$$

where

$$M_3(t) = 1 - \left| \frac{\|f_1^*(t)\| - \|f_2^*(t)\|}{\|F_{\text{sum}}(t)\|} \right|.$$

A higher value of the index indicates more symmetry between the effective forces. The index is suitably bounded between zero and one ($0 \leq I_3 \leq 1$), see [23].

Average of $\alpha(t)$: The index measures the average value of α during the task and is related to the average of the interaction force. It is defined as

$$I_4 = 1 - \frac{|N_\alpha|}{\mathscr{M}_\alpha} \tag{36}$$

where

$$N_\alpha = \frac{1}{t_f - t_i} \int_{t_i}^{t_f} \left(\alpha(t) - \frac{1}{2} \right) \mathrm{d}t$$

and $\mathscr{M}_\alpha$ is the maximum value of $|N_\alpha|$ for a given set of signals $\alpha(t)$. A higher value of the index is associated with the average value of α closer to 0.5. The index is bounded between zero and one by definition ($0 \leq I_4 \leq 1$).

Average Rate of $\alpha(t)$: The index measures the average rate of the variations of α. It is defined as

$$I_5 = 1 - \frac{N_r}{\mathscr{M}_r} \tag{37}$$

where

$$N_r = \frac{1}{t_f - t_i} \int_{t_i}^{t_f} \|\dot{\alpha}(t)\| \, \mathrm{d}t$$

and $\mathscr{M}_r$ is the maximum value of N_r for a given set of signals $\alpha(t)$. A higher value of the index indicates fewer average variations in α. For instance, $I_5 = 1$ holds only if $\alpha(t) = \text{const}$. The index is bounded between zero and one by definition ($0 \leq I_5 \leq 1$).

REFERENCES

[1] V. A. Hughes *et al.*, "Anthropometric assessment of 10-y changes in body composition in the elderly," *Amer. J. Clinical Nutrition*, vol. 80, no. 2, pp. 475–482, 2004.

[2] P. Szulc, T. J. Beck, F. Marchand, and P. D. Delmas, "Low skeletal muscle mass is associated with poor structural parameters of bone and impaired balance in elderly men—The Minos study," *J. Bone Mineral Res.*, vol. 20, no. 5, pp. 721–729, 2005.

[3] D. Williams and O. Khatib, "The virtual linkage: A model for internal forces in multi-grasp manipulation," in *Proc. IEEE Int. Conf. Robot. Autom.*, 1993, pp. 1025–1030.

[4] R. Groten *et al.*, "Experimental analysis of dominance in haptic collaboration," in *Proc. 18th IEEE Int. Symp. Robot Human Interactive Commun.*, 2009, pp. 723–729.

[5] M. Rahman, R. Ikeura, and K. Mizutani, "Control characteristics of two humans in cooperative task and its application to robot control," in *Proc. 26th Annu. Conf. IEEE Ind. Electron. Soc.*, 2000, vol. 3, pp. 1773–1778.

[6] P. Evrard and A. Kheddar, "Homotopy switching model for dyad haptic interaction in physical collaborative tasks," in *Proc. 3rd Joint EuroHaptics Conf. Symp. Haptic Interfaces Virtual Environ. Teleoperator Syst. World Haptics*, Mar. 2009, pp. 45–50.

[7] K. B. Reed, M. Peshkin, M. J. Hartmann, J. E. Colgate, and J. Patton, "Kinesthetic interaction," in *Proc. 9th Int. Conf. Rehabil. Robot.*, 2005, pp. 569–574.

[8] F. Lacquaniti, C. Terzuolo, and P. Viviani, "The law relating the kinematic and figural aspects of drawing movements," *Acta Psychologica*, vol. 54, pp. 115–130, 1983.

[9] P. M. Fitts, "The information capacity of the human motor system in controlling the amplitude of movement," *J. Experimental Psychol.*, vol. 47, pp. 381–391, 1954.

[10] E. Todorov, "Optimality principles in sensorimotor control (review)," *Nature Neurosci.*, vol. 7, no. 9, pp. 907–915, 2004.

[11] F. C. Anderson and M. G. Pandy, "Dynamic optimization of human walking," *J. Biomech. Eng.*, vol. 123, no. 5, pp. 381–390, 2001.

[12] T. Flash and N. Hogan, "The coordination of arm movements: An experimentally confirmed mathematical model," *J. Neurosci.*, vol. 5, no. 7, pp. 1688–1703, 1985.

[13] Y. Uno, M. Kawato, and R. Suzuki, "Formation and control of optimal trajectory in human multijoint arm movement. Minimum torque-change model," *Biol. Cybern.*, vol. 61, pp. 89–101, 1989.

[14] E. Nakano *et al.*, "Quantitative examinations of internal representations for arm trajectory planning: Minimum commanded torque change model," *J. Neurophysiology*, vol. 81, no. 5, pp. 2140–2155, 1999.

[15] C. M. Harris and D. M. Wolpert, "Signal-dependent noise determines motor planning," *Nature*, vol. 394, pp. 780–784, 1998.

[16] J. Tresilian and G. Stelmach, "Common organization for unimanual and bimanual reach-to-grasp tasks," *Exp. Brain Res.*, vol. 115, no. 2, pp. 283–299, 1997.

[17] G. Garvin, M. Žefran, E. Henis, and V. Kumar, "Two-arm trajectory planning in a manipulation task," *Biol. Cybern.*, vol. 76, no. 1, pp. 53–62, 1997.

[18] J. Diedrichsen, "Optimal task-dependent changes of bimanual feedback control and adaptation," *Current Biol.*, vol. 17, no. 19, pp. 1675–1679, 2007.

[19] E. Noohi, S. Parastegari, and M. Žefran, "Computational model for dyadic and bimanual reaching movement," in *Proc. IEEE World Haptics Conf.*, 2015, pp. 260–265.

[20] C. Basdogan, C.-H. Ho, M. A. Srinivasan, and M. Slater, "An experimental study on the role of touch in shared virtual environments," *ACM Trans. Comput.-Human Interaction*, vol. 7, no. 4, pp. 443–460, 2000.

[21] Y. Guiard, "Asymmetric division of labor in human skilled bimanual action: The kinematic chain as a model," *J. Motor Behavior*, vol. 19, no. 4, pp. 486–517, 1987.

[22] K. Reed, M. Peshkin, M. J. Hartmann, M. Grabowecky, J. Patton, and P. M. Vishton, "Haptically linked dyads: Are two motor-control systems better than one?" *Psychological Sci.*, vol. 17, no. 5, pp. 365–366, 2006.

[23] E. Noohi and M. Žefran, "Quantitative measures of cooperation for a dyadic physical interaction task," in *Proc. 14th IEEE-RAS Int. Conf. Humanoid Robots*, 2014, pp. 469–474.

[24] R. Groten, D. Feth, R. L. Klatzky, and A. Peer, "The role of haptic feedback for the integration of intentions in shared task execution," *IEEE Trans. Haptics*, vol. 6, no. 1, pp. 94–105, 2013.

[25] G. Ganesh *et al.*, "Two is better than one: Physical interactions improve motor performance in humans," *Sci. Rep.*, vol. 4, 2014, Art. no. 3824.

[26] R. P. van der Wel, G. Knoblich, and N. Sebanz, "Let the force be with us: Dyads exploit haptic coupling for coordination," *J. Exp. Psychol.: Human Perception Perform.*, vol. 37, no. 5, pp. 1420–1431, 2011.

[27] A. Mörtl *et al.*, "The role of roles: Physical cooperation between humans and robots," *Int. J. Robot. Res.*, vol. 31, no. 13, pp. 1656–1674, 2012.

[28] D. Feth, R. Groten, A. Peer, S. Hirche, and M. Buss, "Performance related energy exchange in haptic human-human interaction in a shared virtual object manipulation task," in *Proc. World Haptics 3rd Joint EuroHaptics Conf. Symp. Haptic Interfaces Virtual Environ. Teleoperator Syst.*, 2009, pp. 338–343.

[29] A. Sawers and L. H. Ting, "Perspectives on human-human sensorimotor interactions for the design of rehabilitation robots," *J. Neuroeng. Rehabil.*, vol. 11, no. 1, 2014, Art. no. 142.

[30] B. Corteville, E. Aertbeliën, H. Bruyninckx, J. De Schutter, and H. Van Brussel, "Human-inspired robot assistant for fast point-to-point movements," in *Proc. IEEE Int. Conf. Robot. Autom.*, 2007, pp. 3639–3644.

[31] A. Bussy, A. Kheddar, A. Crosnier, and F. Keith, "Human-humanoid haptic joint object transportation case study," in *Proc. IEEE/RSJ Int. Conf. Intell. Robots Syst.*, Oct. 2012, pp. 3633–3638.

[32] J. R. Medina, D. Lee, and S. Hirche, "Risk-sensitive optimal feedback control for haptic assistance," in *Proc. IEEE Int. Conf. Robot. Autom.*, 2012, pp. 1025–1031.

[33] S. M. Waller and J. Whitall, "Bilateral arm training: Why and who benefits?" *NeuroRehabilitation*, vol. 23, pp. 29–41, 2008.

[34] R. Shadmehr and F. A. Mussa-Ivaldi, "Adaptive representation of dynamics during learning of a motor task," *J. Neurosci.*, vol. 14, no. 5, pp. 3208–3224, 1994.

[35] T. Flash and I. Gurevich, "Models of motor adaptation and impedance control in human arm movements," *Adv. Psychology*, vol. 119, pp. 423–481, 1997.

[36] A. Melendez-Calderon, M. Fisher, M. Tan, E. Burdet, and J. L. Patton, "Acquisition of motor skills in isometric conditions through synesthetic illusions of movement," in *Proc. IEEE World Haptics Conf.*, 2015, pp. 428–433.

[37] R. Shadmehr and S. P. Wise, *The Computational Neurobiology of Reaching and Pointing: A Foundation for Motor Learning*. Cambridge, MA, USA: MIT Press, 2005.

[38] D. J. Reinkensmeyer, P. S. Lum, and S. L. Lehman, "Human control of a simple two-hand grasp," *Biol. Cybern.*, vol. 67, no. 6, pp. 553–564, 1992.

[39] M. Uchiyama and P. Dauchez, "A symmetric hybrid position/force control scheme for the coordination of two robots," in *Proc. IEEE Int. Conf. Robot. Autom.*, 1988, pp. 350–356.

[40] *F/T Sensor: Gamma*. ATI Industrial Automation, 2014. [Online]. Available: http://www.ati-ia.com/products/ft/ft_models.aspx?id=Gamma.

[41] *NI PCI-6034E (Legacy)*. National Instruments, 2014. [Online]. Available: http://sine.ni.com/nips/cds/view/p/lang/en/nid/11916.

[42] *9 Degrees of Freedom - Sensor Stick*. Sparkfun, 2014. [Online]. Available: https://www.sparkfun.com/products/10724.

[43] *Arduino Mega*. Arduino, 2014. [Online]. Available: http://arduino.cc/en/Main/arduinoBoardMega.
[44] P. N. Sabes, M. I. Jordan, and D. M. Wolpert, "The role of inertial sensitivity in motor planning," *J. Neurosci.*, vol. 18, no. 15, pp. 5948–5957, 1998.
[45] F. Crevecoeur, J.-L. Thonnard, and P. Lefèvre, "Optimal integration of gravity in trajectory planning of vertical pointing movements," *J. Neurophysiology*, vol. 102, no. 2, pp. 786–796, 2009.
[46] *The WAM Arm*. Barrett, 2015. [Online]. Available: http://www.barrett.com/products-arm.htm.

Ehsan Noohi received the B.S. degree in electrical engineering from University of Tehran, Tehran, Iran; the M.S. degree in control engineering from K. N. Toosi University of Technology, Tehran, Iran; and the Ph.D. degree in electrical engineering from University of Tehran, Tehran. He is currently working toward the Ph.D. degree at the Department of Electrical and Computer Engineering, University of Illinois at Chicago, Chicago, IL, USA.

He is also a Visiting Researcher with the Robotics Laboratory, Rehabilitation Institute of Chicago, Chicago, IL, USA. His research interests include robotics, modeling and control of wheel-based manipulators, modeling human–human manipulative interactions, modeling and control of human–robot physical interaction, and haptics.

Miloš Žefran received the Undergraduate degree in electrical engineering and mathematics at University of Ljubljana, Ljubljana, Slovenia, where he also received the M.Sc. degree in electrical engineering. He received the M.Sc. degree in mechanical engineering and the Ph.D. degree in computer and information science in 1995 and 1996, respectively, from University of Pennsylvania, Philadelphia, PA, USA.

From 1997 to 1999 he was an National Science Foundation (NSF) Postdoctoral Scholar with California Institute of Technology, Pasadena, CA, USA. He then joined Rensselaer Polytechnic Institute, Troy, NY, USA. Since 1999 he has been with the Department of Electrical and Computer Engineering, University of Illinois at Chicago, where he is a Professor and the Director of Graduate Studies. In 2008 he was a Visiting Researcher with University of Pisa, Pisa, Italy. His research interests include robotics and control with applications to human–robot interaction, cyber–physical systems, and robot networks. His research has been supported by the NSF Career Award in 2000 and a number of subsequent NSF awards. He has published more than 100 journal and conference papers and is the Associate Editor for IEEE TRANSACTIONS ON CONTROL SYSTEMS TECHNOLOGY.

James L. Patton received the B.S. degree in mechanical engineering and engineering science from University of Michigan, Ann Arbor, MI, USA; the M.S. degree in theoretical mechanics from Michigan State University, East Lansing, MI, USA; and the Ph.D. degree in biomedical engineering from Northwestern University, Evanston, IL, USA.

He currently is a Professor of bioengineering with University of Illinois at Chicago, Chicago, IL, USA, and an Associate Director of the Center for Rehabilitation Robotics, Rehabilitation Institute of Chicago, Chicago, IL, USA. He also holds affiliate positions in Physical Medicine and Rehabilitation and Mechanical and Biomedical Engineering with Northwestern University. He has worked in manufacturing for Ford and as a Cyclotron Operator in nuclear medicine before turning his attention to biomechanics and control of human movement. His general interests include robotic teaching, dynamic balance control, haptics, modeling of the human–machine interface, and robot-facilitated recovery from a brain injury. His research has demonstrated how control is made robust by avoiding undesirable situations. His more recent research has demonstrated how one can exploit the nervous system's natural capacity to adapt in order to teach movements and help people to recover from brain injury. He is on the International Advisory Committee for the IEEE-EMBS and also chairs the technical committee on biomedical robotics.